J. Astrophys. Astr. (December 2017) 38:72
https://doi.org/10.1007/s12036-017-9492-3

Identification of Stellar Sequences in Various Stellar Systems: ESO65-SC03, Teutsch 106, Turner 6

GIREESH C. JOSHI

Department of Physics, Kumaun University, Nainital, Uttarakhand 263 001, India.
E-mail: gchandra.2012@rediffmail.com

MS received 17 July 2017; accepted 23 October 2017; published online 27 November 2017

Abstract. The spatial morphological study of stellar clusters has been carried out through their identified probable members. The field stars decontamination is performed by the statistical cleaning approach (depends on the magnitude and colour of stars within the field and cluster regions). The colour magnitude ratio diagram (CMRD) approach is used to separate the stellar sequences of cluster systems. The age, distance and reddening of each cluster is estimated through the visual inspection of best fitted isochrone in colour magnitude diagrams (CMDs). The mean proper motion values of stellar clusters are obtained through the extracted data from PPMXL and UCAC4 catalogs. Moreover, these values vary according to the extracted data-set from these catalogues. This variation has occurred due to different estimation efficiency of proper motions. The two colour ratio (TCR) and two colour magnitude ratio (TCMR) values of each cluster is determined by utilizing the WISE and PPMXL catalogues, these values are found abnormal for Teutsch 106. In addition, the TCMR values are similar to TCR values at longer wavelength, whereas both values are far away from each other at shorter wavelength. The fraction of young stellar objects (YSOs) is also computed for each cluster.

Keywords. Methods: analytical—data analysis—techniques: photometric—catalogues—open stellar clusters: individual.

1. Introduction

The open stellar clusters (OCs) are distributed in the galactic plane of spiral and irregular galaxies. These objects are used for the stellar and galactic investigations (Hasan 2005 and references within it). Since OCs are formed by the collapse and fragmentation of a turbulent molecular cloud (Harris & Pudritz 1994; Bate *et al.* 2003), they become ready samples to study the stellar evolution history. OCs are also used to constraint the stellar formation processes in the Galactic disk (Dias *et al.* 2012). Such studies are easily carried out by CMDs due to stars having the same distance, chemical composition and age; but having different mass (Friel 1995; Hasan *et al.* 2008). OCs are dynamic and loosely gravitational bound systems (Joshi & Tyagi 2015). Generally, these objects are identified due to their stellar enhanced compared to the nearby sky. They are also disrupted at the time of revolving around the Galactic center through close encounters with another neighbour cluster and clouds of gas. Thus, the stellar density of any cluster decreases with time due to the dispersion and internal close encounters of its members. The OCs can be divided into dense and sparse OCs according to their stellar density. The main sequence (MS) of sparse one is easily identified as compared to dense ones. Moreover, the estimation accuracy of parameters of OSC depends on the identified MS. Thus, each cluster shows unique stellar sequence (i.e. MS) of dynamical stars. There are several examples of the CMDs of stellar clusters such as, NGC 4755 (Bonatto *et al.* 2006), M11 (Santos *et al.* 2005) having apparent stellar sequences more than one. One of these sequences is referred as the MS of studied cluster, whereas other may be the sub- or red-giant branch. The cluster's parameter dependency on stellar sequence may be understood through the comparative study of some sparse and dense stellar clusters. Joshi & Tyagi (2016) have proposed the colour-magnitude ratio diagram method (CMRD) for separating the stellar sequences and stellar membership of stellar clusters. In this connection, the CMRD method has been used for the membership estimation of stellar clusters. Here, the spatial morphological study of a cluster remnant [ESO 65 03 (Joshi *et al.* 2015)] and one dense cluster regions

Table 1. The different literature coordinates of the stellar clusters.

Literature	ESO65-SC03 (RA & DEC)	Turner 6 (RA & DEC)	Teutsch 106 (RA & DEC)
Kharchenko *et al.* (2013)	12:51:18	10:59:01	10:59:25.1
	−69:43:48	−59:28:59	−59:32:06
Dias *et al.* (2014)	12:51:37	10:59:01	10:59:25
	−69:43:48	−59:29:58	−59:32:49
Joshi *et al.* (2015)	12:51:19.7	—	—
	−69:43:21.6	—	—
Froebrich (2010)	—	10:59:25.1	—
	—	−59:32:12	—

(Turner 6 + Teutsch 106) has been presented. These stellar clusters are listed on SIMBAD[1] website, which has provided the stellar cluster database of studied and poorly studied stellar clusters. The data-sets of presently studied stellar clusters have been extracted from the PPMXL (Roëser *et al.* 2010), UCAC4 (Zacharias *et al.* 2013) and WISE (Wright *et al.* 2010) catalogues.

The present manuscript is organized as follows. The previous studies of stellar clusters are described in section 2. The existence of stellar clusters is discussed in section 3. The parametric results are estimated in section 4. Sections 5 and 6 are devoted to two colour-magnitude ratio diagrams and identification of young stellar objects, respectively. The final conclusion and discussion are stated in section 7.

2. Known parameters of star clusters

In the present sample of stellar clusters, we have taken one cluster remnant (ESO65 SC03 or ESO 65 03) and one dense cluster region (Turner 6 + Teutsch 106). The selected dense cluster regions has covered the field region of both stellar clusters namely, Turner 6 and Teutsch 106. These stellar systems are situated at the southern hemisphere of the sky. Dias *et al.* (2002, 2014) and Kharchenko *et al.* (2013) have compiled the catalogues for the optically visible stellar clusters and candidates. The various heterogeneous parametric results of studied stellar clusters are found in literature, which is described as following. The center coordinates of Turner 6 is given by Froebrich (2010) as $10^h59^m25.1^s$, $-59^o32'12''$, which are very close to center coordinate given by Dias *et al.* (2014) catalogue and Kharchenko *et al.* (2013) catalogue, for Teutsch 106 such as $10^h59^m25.0^s$, $-59^o32'49''$ and $10^h59^m25.1^s$, $-59^o32'06''$ respectively. Similarly, the center coordinates of Turner 6 are extracted from both catalogs as $10^h59^m01.0^s$, $-59^o29'58''$ and $10^h59^m01.0^s$, $-59^o28'59''$ respectively. Moreover, the estimated cluster radius of Turner 6 and Teutsch 106 is 1.65 arcmin (Bonatto & Bica 2010; Dias *et al.* 2014) and 2.60 arcmin (Tadross 2009; Dias *et al.* 2014) respectively. The center, core-radius and radius of ESO-65SC03 has also been estimated by Kharchenko *et al.* (2013) as $12^h51^m18^s$, $-69^o43'48.0''$, 1.5 arcmin and 8.4 arcmin respectively, whereas Dias *et al.* (2014) reported that the center and radius of this systems are to be $12^h51^m\ 37^s.0$, $-69^o43'48''$ and 3 arcmin respectively. Joshi *et al.* (2015) have declared that ESO-65SC03 is a cluster remnant. According to their analysis, the center of this system is found to be $\alpha = 12^h : 51^m : 19.7^s, \delta = -69^o : 43' : 21.6''$. All these results of studied stellar clusters are listed in Table 1.

3. Stellar sequences and membership of stellar clusters

The stellar distribution of CMD is an excellent tool to identify the stellar sequences. The stellar evolution process depends on their initial mass and they are identical to similar luminous stars of cluster. Field star sequences (FSS) is also associated with the MS of OCs. Moreover, the stellar density of FSS is limited to some magnitude range towards the fainter end. These field stars can be separated from the members of cluster through the statistical approach (Joshi *et al.* 2014) and membership criteria on the kinematic probabilities (Zhao & Shao 1994; Yadav *et al.* 2013). In the statistical approach, the field stars decontamination is carried out according

[1] http://simbad.u-strasbg.fr/guide/index.htx.

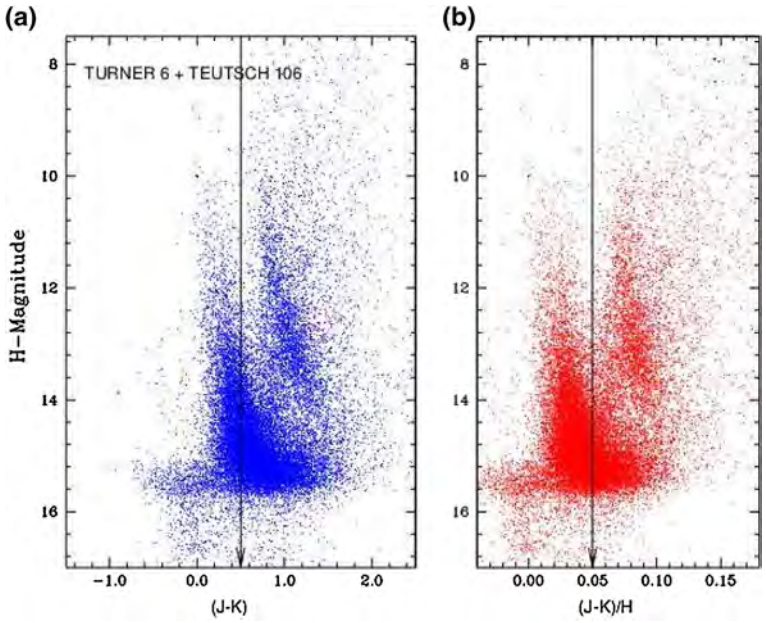

Figure 1. (**a**) and (**b**) represent the $(J-K)$ vs. H CMD and $(J-K)/H$ vs. H CMRD for dense cluster regions of Turner 6+ Teutsch 106. The arrows in (a) represent the value of $(J-K)$ (0.5 for Turner 6 + Teutsch 106). Similarly, the arrows in (b) represent the values of CMR, i.e. $(J-K)/H$ (0.05 for Turner 6 + Teutsch 106 region). The arrow in (b) is used to separate the star sequences within the dense cluster region.

to their colour and magnitude dissimilarities from the members of OSC. The membership probability also depends on the proper motion of these members. Joshi *et al.* (2015) have reported that the field sequence may still be present in CMDs after field star decontamination through the statistical cleaning approach. The presence of field stars also influences the stellar distribution and estimation precision of cluster's parameters. In some cases, the stellar density of two identified sequences of an OSC is so much similar that it is difficult to decide actual MS. Since, such type pattern of stellar sequences can also be produced by the field stars, the well-known catalogued stellar clusters are studied. We have discussed some examples of OSC in the previous section, in which two stellar sequences are noticed in a single $(J-H)$ vs. K CMD of a cluster. In addition, the parameters of OSC are estimated through the fitting of theoretical isochrones on these CMDs. These model fit is/may bend at the fainter limit of stellar magnitudes and leads to a false estimation of distance and reddening values of the cluster due to the overlapping of different stellar sequences. Thus, a new approach is required to distinguish these stellar sequences before estimating the cluster's parameters. Since the normal CMD is not suitable for this purpose, CMRD method (Joshi & Tyagi 2016) has been applied.

To reduce broadening effect of linear trend of colours with magnitude, we have normalized stellar colour values with their magnitude. These colour-normalized values (colour magnitude ratio, i.e. CMR) are taken instead of colours in CMD. In the present case of Teutsch 106 and Turner 6 (T106 + T6), the stellar sub-sequence seems to be less dense compared to the MS. To reduce the broadening effect, the CMR diagram (CMRD) method is applied for analyzing it. In the CMRD, X-axis and Y-axis represent H magnitude of stars and corresponding $(J-K)/H$ ratio respectively. In Fig. 1 (**a**), (**b**), the CMD and CMRD are plotted for T106 + T6 region in left and right panels, respectively. The CMRD contains two stellar sequences, which are distinguished by a constant colour-magnitude ratio (CMR) value, i.e., 0.05. This value (0.05) is marked by a black arrow in Fig. 1. The separated sequences of T106 + T6 region are clearly shown on the CMD and CMRD diagrams. Thus, CMRD is an excellent tool to estimate the cluster parameters. The advantage of CMRD are given below:

(i) The membership uncertainty of stars of OSC is greater in magnitude due to the fact that stars of higher magnitude show more scattering on the CMD plane. Such scattering is relatively low for CMRD.
(ii) The CMRD plane shows more clear separation for stellar sequences compare to CMD.

(iii) It is clear from Fig. 1 that the separation magnitude range is increased in the CMRD compared to CMD. For example, the separation-range of stellar sequences of T106 + T6 region is $7.6 - 12.8 \pm 0.4$ H-mag on the plane of CMD, whereas this range increases as $7.6 - 14.4 \pm 0.4$ H-mag on the plane of CMRD.

(iv) A solution of linear equation is needed to separate the stellar sequences of CMD, whereas this separation is possible through a constant value of the colour-magnitude ratio of CMRD.

4. Parameter estimation

The spatial characteristic and dynamical behaviour of a cluster is understood through the precise estimation of cluster's parameters such as distance, age, radius, mean proper motion and reddening. In the present study of stellar clusters these parameters are estimated through the extracted data from the PPMXL catalog (Roëser *et al.* 2010). This catalog provides the stellar RA–DEC coordinates. The estimation procedure of various parameters of stellar clusters are given in the following sub-sections.

4.1 *Center, core radius, radius and limit radius*

The radial size of an OSC is defined in terms of projected radius. The radius can be determined through the radial density profile (RDP) of the cluster. The exact RDP and accurate center of any OSC are not obtained due to irregular shape and non-uniform distribution of stars at different brightness levels (Joshi *et al.* 2014). The cluster's center holds maximum stellar density in whole cluster region and identified through the stellar distribution of OCs on RA–DEC plane. Similarly, the RDP of each cluster is constructed for calculating their radius. For this purpose, the cluster region is divided into concentric rings, from the cluster's center and the stellar density of each ring is determined by dividing the total number of stars in the ring by its area. The RDP of each cluster is obtained by fitting of a model (Kaluzny & Udalski 1992) on the RDP of a cluster. The projected radial density $\rho(r)$ of each cluster is estimated by the following model:

$$\rho(r) = \rho(0) + \frac{f_0}{1 + (\frac{r}{r_c})^2}, \tag{1}$$

where r_c is the core radius of cluster. This core radius is defined as the radial distance from the cluster's center where the stellar density reduce half of the central/peak density f_0 above the background stellar density $\rho(0)$. The constructed RDP of each cluster is shown in Figures 2(a)–(d) (as obtained through PPMXL catalogue). The straight line of each panel represents the $\rho(b)$, which is intercepted to the RDP of each cluster. The distance of this intercept point from the origin (cluster center) is defined as the cluster's radius. The continuous decrements of stellar density is found in RDP of the cluster from origin to intercept point and no stellar density decrements appears after this point. The stellar density after this point is known as the borderline background stellar density (ρ_b), which is co-related to the model $\rho(0)$ by the following mathematical expression,

$$\rho_b = \rho_0 + 3\sigma_{bg} \tag{2}$$

where σ_{bg} is the uncertainty in the estimation of ρ_0. However, the cluster extent is also determined in terms of model limiting radius ($r_{\rm limit}$). This radius represents the weak gravitational bounded region of the cluster (Joshi *et al.* 2015) and estimated by the following relation (Bukowiecki *et al.* 2011):

$$r_{\rm limit} = r_c \sqrt{\frac{f_0}{3\sigma_{bg}} - 1}. \tag{3}$$

Furthermore, this limit radius is used to estimate the cluster's concentric parameter (c) by the following relation (Peterson & King 1975):

$$c = \log\left(\frac{r_{\rm limit}}{r_c}\right). \tag{4}$$

These prescribed parameters of each cluster are briefly described as follows and also summarized in Table 2. In this Table, the peak density f_0 is the difference between the value of the y-intercept of the model and the background stellar density ρ_0.

4.1.1 *ESO-65SC03.* The new center-coordinates are ($12^{\rm h}51^{\rm m}11^{\rm s}.5$, $-69^{\rm o}42'34.2''$) with the uncertainty of $5''$. The RDP of this cluster is constructed from the data-points of stellar densities of concentric ring of 1.0 arcmin width. The core radius, radius and limit radius of cluster are found to be 1.3 ± 0.2 arcmin, 5.0 ± 0.2 arcmin and 5.48 arcmin respectively. Its RDP plot is constructed through the PPMXL catalogue, which provides different values compared to the work of 2MASS catalogue (Joshi *et al.* 2015).

4.1.2 *Turner 6 and Teutsch 106.* The RDP of Teutsch 106 region is constructed through the extracted data from the PPMXL catalog. The cluster's center is found to be ($10^{\rm h}59^{\rm m}19^{\rm s}.0$, $-59^{\rm o}32'20.9^{\rm s}$) in RA–DEC plane

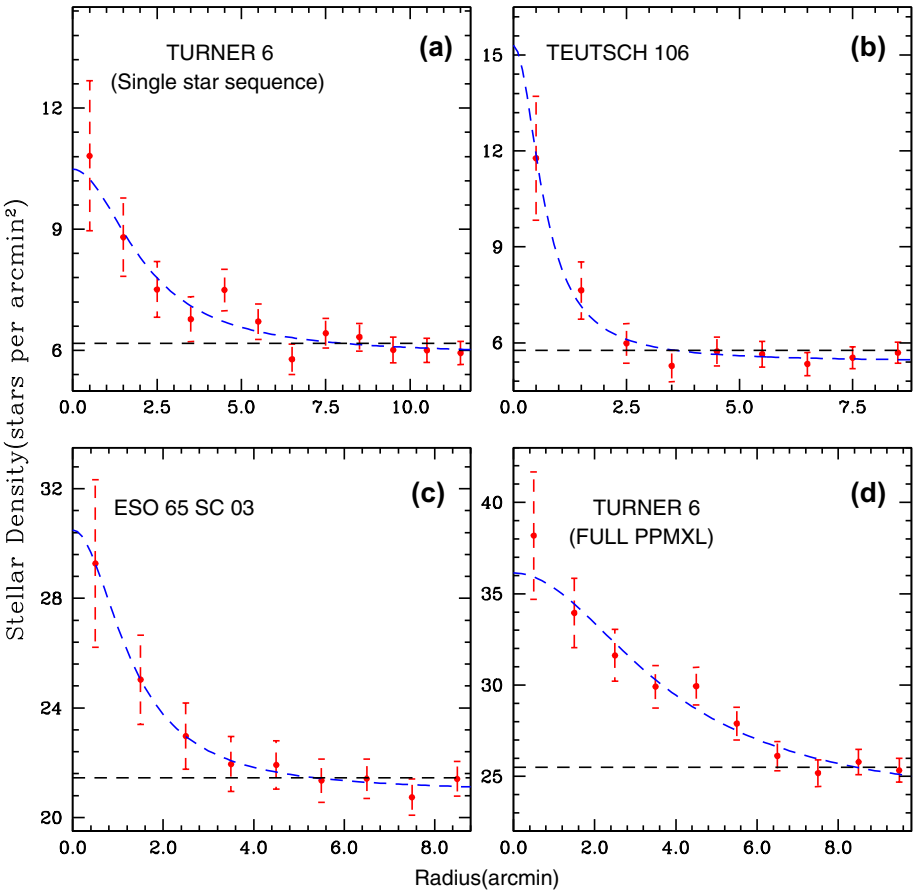

Figure 2 (**a**)–(**d**). The radial density profile (RDP) of stellar clusters through stellar density within concentric rings. The blue dashed line shows the modified king empirical profile while black dashed line shows the field density. The error of density estimation is calculated by the relation $\sigma_i = \frac{\sqrt{N_i}}{A_i}$, where N_i is the total number of stars present in an area A_i.

Table 2. The various spatial parameters such as, radius, limit radius, etc. have been summarized in this table.

Parameter↓/Cluster→	ESO65-SC03	Teutsch 106	Turner 6
RA (center)	$12^h51^m11^s.5$	$10^h59^m23^s.3$	$10^h58^m47^s.1$
DEC (center)	$-69^o42'34.2''$	$-59^o32'36.9''$	$-59^o34'22.1''$
r_c (arcmin)	1.30	0.69 ± 0.23	2.11 ± 0.58
ρ_0	20.91	5.41 ± 0.12	5.87 ± 0.10
σ_{bg}	0.17	0.12	0.10
ρ_b	21.42	5.77	6.17
Peak density	9.58 ± 1.52	9.89 ± 3.53	4.61 ± 1.25
Radius (arcmin)	5.0	3.5	8.5
r_{limit} (arcmin)	5.48	3.55	9.09
c	0.62	0.71	0.63

through the maximum count method (Joshi *et al.* 2015) which is close to the coordinates given by Froebrich (2010) and Dias *et al.* (2014) for Turner 6 and Teutsch 106 respectively. In addition, the core radius and radius of this cluster is estimated to be 4.18 ± 0.77 arcmin and 8.5 arcmin respectively. Thus, computed radius is found to be higher than the given radius in literature. In addition, the different stellar sequences (as founded by CMRD approach) are also used for this purpose. The stellar sequence (having a CMR value less than 0.5)

referred as the Teutsch 106 is due to the most recent naming of stellar clusters and its results. The center, core-radius, radius and limit radius for Teutsch 106 are found to be ($10^h59^m23^s.3$, $-59^o32'36.9''$), 0.69 ± 0.23 arcmin, 3.5 arcmin and 3.55 arcmin respectively. The second stellar sequence referred to as the Turner 6 and its best RDP is obtained by those stars which are spread out in whole cluster region. The center, core-radius, radius and limit radius of Turner 6 are found to be ($10^h58^m\ 47^s.1$, $-59^o34'22.1''$), $2.11 \pm 0.58'$, $8.5'$ and $9.09'$ respectively.

The RDP plot of Turner 6 (full region) through the PPMXL catalog has also been constructed, which provides an entirely different set of results. The resultant RDPs are depicted in Fig. 2.

4.2 *Probable members and mean proper motion*

Mean proper motion of stellar clusters is an angular displacement rate and it measures in the unit of mili-arc sec (mas) per year. The symbols μ_x and μ_y represent the stellar proper motion in RA and DEC directions, respectively. The values of stellar proper-motion of the stellar clusters' members are extracted from PPMXL catalog. This catalog provides a list of about 900 million stars with an accuracy of 80−300 mas in stellar coordinate and 4–10 mas per year in the absolute proper motion and also has the completeness of stars at fainter limit.

The probable members of the cluster have been obtained through the combined effort of the CMRD and statistical cleaning approach. In the later approach, the area of field region is taken to be equal to the area of the cluster. Furthermore, we are constructing a grid cell of each field star in the colour-magnitude space. That star of cluster region is rejected from its membership, which is lying in grid-cell of field star and having minimum color-magnitude distance from the star field. Since, the grid size of field stars depend on the stellar density of the cluster, smaller cells are accepted in dense stellar clusters while larger ones for the sparse ones (Corradi *et al.* 2009). These probable members are used to determine the mean proper motion of the cluster by using the iteration method (Joshi *et al.* 2014, 2015). In this method, the mean and standard deviation (σ) values of proper motion of the cluster's members are determined in both right accession (RA) and declination (DEC) directions and rejected membership of those stars which are laying outside the 3σ value of the mean proper motion of any direction. The whole procedure is repeated until all stars are not lying within the 3σ value of the said mean in both directions. The left members are used to determine the mean proper motion of individual cluster (as depicted in RA–DEC plane by blue dots in Fig. 3 (a)–(c)).

The proper motions of stars of stellar sequences of OCs are extracted from the PPMXL catalogue. After applying the CMRD approach, the number of extracted data-points are found to be 450, 285 and 1252 stars for ESO 65, 03, Teutsch 106 and Turner 6 respectively. After applying the statistical cleaning approach, we found 170, 178 and 422 members for the ESO 65 03, Teutsch 106 and Turner 6 respectively. The iteration method of σ-clipping algorithm are provided by the mean proper motion of 139, 171 and 395 members for ESO 65 03, Teutsch 106 and Turner 6 respectively. The resultant values of mean proper motion are listed in Table 3. These results show close agreement with the (Kharchenko *et al.* 2013). The corresponding mean proper values of stellar clusters through UCAC4 catalog are also summarized in Table 3.

In addition, the mean proper motion for Turner 6 (full sky region of cluster) is found to be $\bar{\mu}_x = -0.72 \pm 0.69$ and $\bar{\mu}_y = 0.37 \pm 0.71$ in RA and DEC directions respectively. These values are determined through the proper motion values of the 1959 members of Turner 6, which are left after σ-clipping algorithm on the all 2163 identified members in the described region.

4.3 *CMD: Distance and age*

The stellar broadening is found on CMDs due to the presence of probable binaries and field stars (Sharma *et al.* 2006). However, the stars of MS of CMDs are excellent tools to estimate the physical parameters (distance, age, reddening etc.) of stellar clusters. These parameters can be obtained for the stellar clusters by best fitted theoretical isochrones. These isochrones are based on model dependent mass, radius and distance of each star. Since the near-Infrared surveys of stellar clusters are less affected by high reddening from the Galactic plane, they are selected to estimate the stellar clusters' parameters. The field star decontamination are already carried out in the previous section. The identified probable members are also utilized to determine the distance and age of the stellar clusters. These parameters are estimated by visual inspection of best fitted isochrones on cluster CMDs, which is obtained by checking the several Padova group isochrones of stellar evolution model (Marigo *et al.* 2008; Girardi *et al.* 2010). The best fitted isochrones provide fixed values of colour excess. The distance and age of star clusters are estimated by keeping the fixed value of colour excess $(J-H)$ and $(H-K)$ on H vs. $(J-H)$ and H vs.

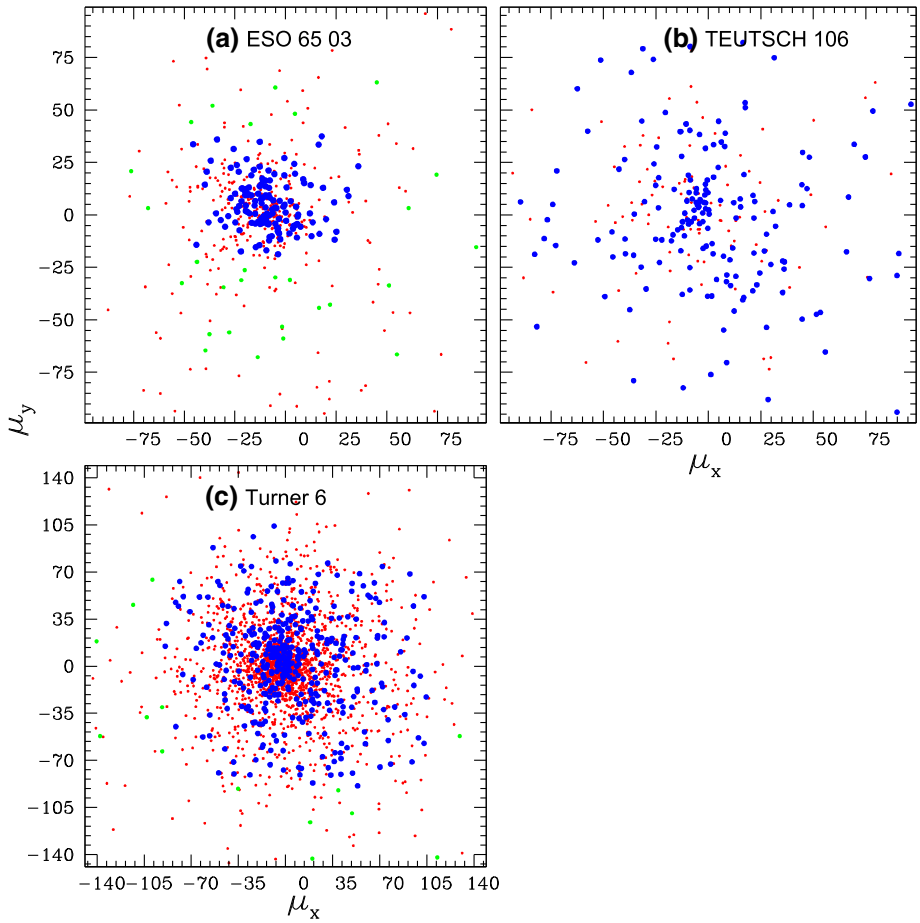

Figure 3 (**a**)–(**c**). The distribution of stars in the $\mu_x - \mu_y$ plane, have been used to estimate the mean proper motion of the cluster. The red, green and blue dots are depicted as detected stars, the remaining members through the CMRD separation and final members through the proper motions.

$(H-K)$ CMDs in such a manner that the colour-excess values should obey the relations of Fiorucci & Munari (2003) for normal interstellar medium. The relations of Fiorucci & Munari (2003) are used to verify the colour excess values as estimated by best-fitted isochrones due to the fact that their work has been co-related to the values of colour excess $(J-H)$ and $(H-K)$ in near infra-red photometry. The distance of a cluster is estimated by the following relation:

$$\text{Distance (kpc)} = 10^{1+\frac{H-A_H}{5}}, \quad (5)$$

where H is the total cluster H-band magnitude and A_H is extinction in H band which has been found by the relation $A_{\rm H} = 0.176A_V$ (Schlegel *et al.* 1998) and $A_V = R_V E(B-V) = 3.1E(B-V)$ (Schlegel *et al.* 1998). The value of reddening, i.e. $E(B-V)$, is estimated by the relation $E(J-H)/E(B-V) = 0.31 \pm 0.13$ (Fiorucci & Munari 2003). The results of age and distance of each cluster are described in the following/next sub-section.

Table 3. The cluster's mean proper motion values in RA and DEC direction using PPMXL and UCAC4 have been listed.

Cluster↓	Catalogue→ Values↓	PPMXL	UCAC4
ESO65-SC03	μ_x	-8.59 ± 1.29	-0.72 ± 0.69
	μ_y	5.29 ± 1.03	0.37 ± 0.71
Teutsch 106	μ_x	-0.78 ± 2.71	-1.13 ± 0.94
	μ_y	-3.11 ± 2.74	-0.93 ± 0.83
Turner 6	μ_x	3.53 ± 1.91	0.04 ± 1.26
	μ_y	1.56 ± 1.89	0.48 ± 1.41

4.3.1 *ESO65-SC03.* In the case of the present studied cluster, the grid size is taken to be $(\pm 0.3, \pm 0.06)$ for statistical approach. The log-age, the total cluster H-band magnitude, distance modulus and colour-excess $(J-H)$ are found to be 8.75 ± 0.05, 12.5 ± 0.1, 12.4 ± 0.1 and 0.15 respectively, which leads to the age, distance and reddening of studied cluster as 0.56 ± 0.01 Gyr, $3.04 \pm$

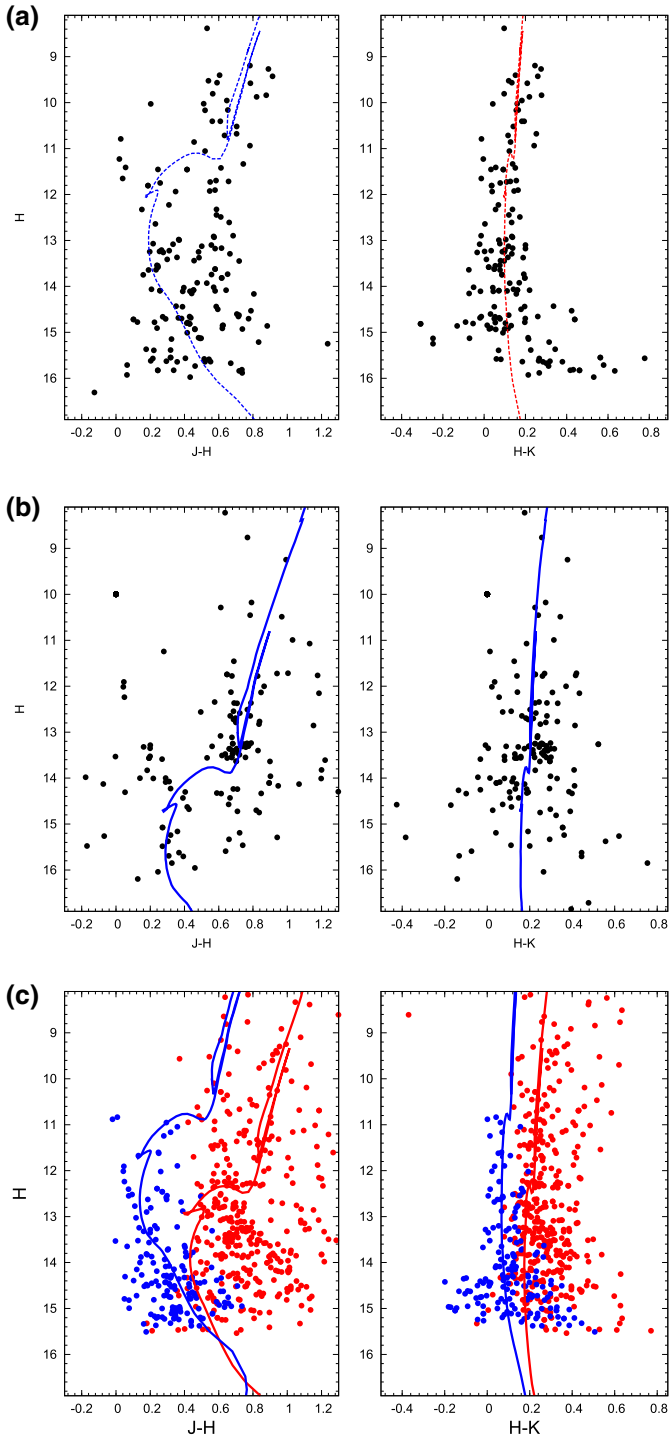

Figure 4. The $(J - H)$ vs. H and $(H - K)$ vs. H CMDs for the studied stellar clusters. The black dots in each panel (excluding panel (c)) represent those stars which remain after field star subtraction from cluster region. The blue and red dots in panel (c) represent the stars of Teutsch 106 and Turner 6 respectively. (**a**) ESO65-SC03. (**b**) Teutsch 106 (statistical cleaned). (**c**) Teutsch 106 and Turner 6.

0.30 kpc and 0.38 respectively. The estimated age is very close to 3.047 kpc as estimated by (Kharchenko *et al.* 2013). The best-fitted isochrone of solar mettallicity is depicted in Fig. 4(a).

4.3.2 *Turner 6 and Teutsch 106.* A typical distance of Teutsch 106 is determined through the same cluster region as selected by Dias *et al.* (2014). The field star decontamination of this region is performed by adopt-

Table 4. The various parameters obtained through CMDs are summarized here.

Cluster/Parameter	Distance modulus (mag)	Age (Gyr)	Distance (kpc)	Reddening (mag)
ESO65SC03	12.42 ± 0.20	0.56 ± 0.05	3.04 ± 0.30	0.38
Turner 6	12.47 ± 0.1	0.89 ± 0.10	3.12 ± 0.03	1.03
Teutsch 106	11.19 ± 0.1	0.79 ± 0.05	1.73 ± 0.02	0.32

ing a grid size (0.2 mag, 0.05 mag) on $(H, J-H)$ CMD. The distance and reddening of Teutsch 106 are determined to be 6.6 kpc and 0.81 mag respectively, which show good agreement with distance 6.7 kpc and reddening 0.97 mag as estimated by Kharchenko *et al.* (2013). It is clear from Fig. 4(b) that the probable members of this region are show broad scatter pattern of stars. These values are obtained by the combined stellar sequences of Turner 6 and Teutsch 106 (hereinafter T106+T6).

On the other hand, statistical cleaned approach (grid size, $(H, (J-H)) = \pm 0.05, \pm 0.05$) are also used to separate both identified stellar sequences through CMRD approach. The age, distance, and reddening of Teutsch 106 are found to be 0.79 ± 0.05 Gyr, 1.73 kpc and 0.32 mag respectively. Thus, these results of age, distance and reddening are far away from the results of Kharchenko *et al.* (2013) and Dias *et al.* (2014). Our selected Teutsch 106 region and T106 + T6 region overlap but have different size. The statistical cleaned CMD of T106 + T6 is not showing different stellar sequences due to the higher rejection of stars by larger grid size. The larger grid size is against the hypothesis of small grid size of dense region. Moreover, larger grid size do not reduces the stellar scattering in CMD. The broader and scattered distribution of stars can become the cause of wrong estimation of visual fit of isochrones on CMD. Since, the parametric results of Teutsch 106 is not matched with the said T106 + T6 region, the analysis of stellar sequences of cluster regions may open a new window of cluster studies.

The distance and reddening of Turner 6 are estimated to be 3.12 kpc and 1.03 mag respectively. Kharchenko *et al.* (2013) also estimated the distance and reddening of this cluster as 3.6 kpc and 1.14 mag respectively. Our results show good agreement with the results of Kharchenko *et al.* (2013). Similarly, the distance of studied cluster is estimated to be 3.25 kpc by Dias *et al.* (2014), which is close to our results. The red and blue lines represent the best fit isochrone of solar and 0.008 metallicity respectively as depicted in Fig. 4(c).

The summary of distance, age and reddening is given in the Table 4.

4.4 *Two-colour diagrams (TCD) and ratios*

Two-colour diagrams (TCD) are useful to determine the reddening and investigating the nature of reddening law in the direction of cluster region. The normal reddening law $R_V = \frac{A_V}{E(B-V)}$ is valid for lines of sights which do not pass through the dense clouds (Sneden *et al.* 1978).

4.4.1 *Reddening through* $(J-K)/(J-H)$ *diagram.* To determine interstellar extinction in the near-IR, the $(J-K)/(J-H)$ diagram is used and depicted in the Fig. 5. We applied the normal reddening law for the infrared colours and shifted the stars along the vector $\frac{E(J-H)}{E(J-K)}$ using different theoretical isochrones (Marigo *et al.* 2008). The relation $E(J-K)/E(B-V) = 0.72 \pm 0.05$ (Morgan & Nandy 1982) is used to estimate the reddening, i.e., $E(B-V)$, for individual cluster. The colour-shifts $(\Delta_{(J-H)}, \Delta_{(J-K)})$ of ESO65-SC03, Teutsch 106 and Turner 6 are found to be (0.26, 0.15), (0.19, 0.12) and (0.61, 0.38) respectively. These shifted values are used to determine the reddening values of ESO65-SC03, Teutsch 106 and Turner 6. The reddening values are 0.36, 0.26 and 0.84 mag respectively. Moreover, these reddening values show good agreement with the values in Table 4.

4.4.2 *Colour-ratios.* Colour ratio values of two colour-diagrams are important for investigating the nature of extinction law, dependency on each other and their variation from normal values (Joshi & Tyagi 2016). The linear relationship of various colours $((H-\lambda)$, where $\lambda = B_{ph}, R_{ph}, I_{ph}, J, W1$ and $W2$ bands) of each cluster are estimated with the colour $(H-K)$. The best linear fit values are listed in Table 5. The colour-ratio results of Teutsch 106 are found to be abnormal compared to other stellar clusters. These abnormal values are interesting puzzles to understand the cause of such variations. These variations may be a due to the presence of molecular cloud/dust, which is also supplemented by mid-IR colours. Furthermore, the values of these ratios are normal for other studied stellar clusters. In addition, $(H-W_1)/(H-K)$ values for ESO65-SC03 and

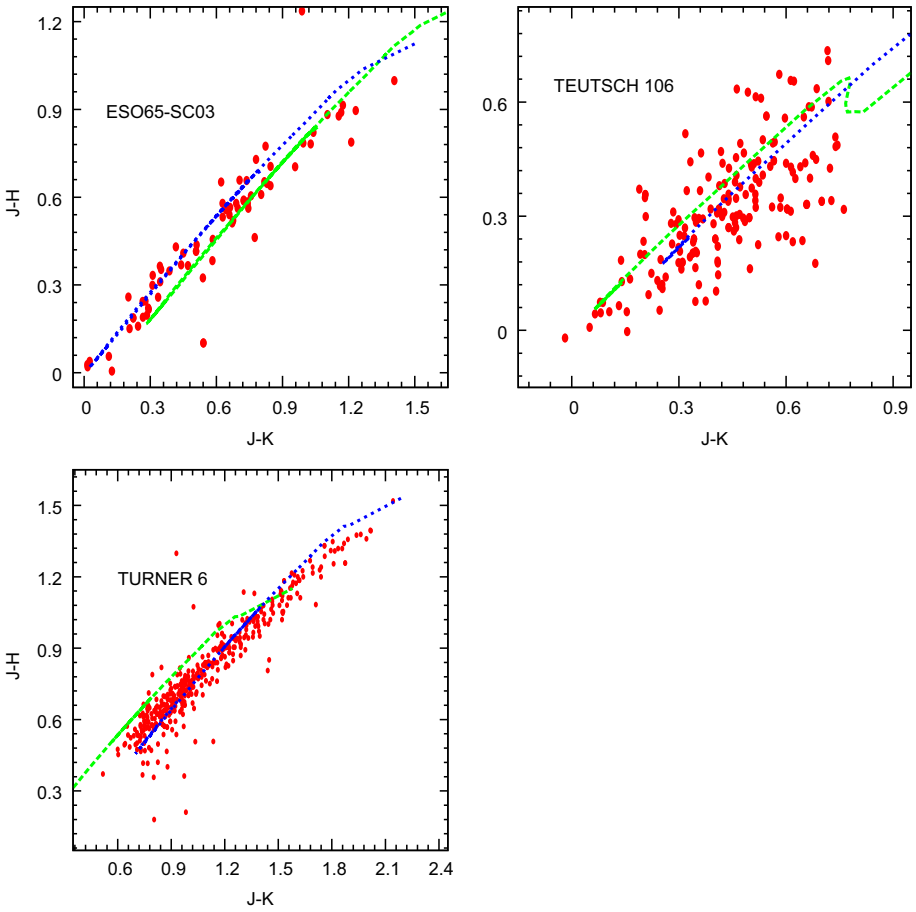

Figure 5. The $(J-K)/(J-H)$ two-colour diagram for stellar clusters.

Table 5. The slopes of the $(H-\lambda)$ versus $(H-K)$ diagrams in the direction of cluster.

Ratios / Cluster	ESO65-SC03	Turner 6	Teutsch 106
$\frac{(H-B_{ph})}{(H-K)}$	-10.57 ± 1.23	-6.66 ± 0.88	4.97 ± 2.58
$\frac{(H-R_{ph})}{(H-K)}$	-7.17 ± 1.17	-7.46 ± 0.75	0.50 ± 3.94
$\frac{(H-I_{ph})}{(H-K)}$	-4.74 ± 0.66	-5.09 ± 0.94	-1.67 ± 2.04
$\frac{(J-H)}{(H-K)}$	1.54 ± 0.19	1.80 ± 0.09	0.10 ± 0.32
$\frac{(H-W_1)}{(H-K)}$	0.89 ± 0.13	1.46 ± 0.10	0.86 ± 0.28
$\frac{(H-W_2)}{(H-K)}$	0.76 ± 0.18	1.53 ± 0.11	0.66 ± 0.42

Teutsch 106 are found more than $(H-W_2)/(H-K)$ whereas the reverse fact is found for Turner 6.

5. Two-colour magnitude ratio diagrams

The colour-magnitude ratio values of CMRD are more effective compared to the colour values of CMD. The stellar scattering of CMD plane is greater than CMRD plane. In this background, a new two-colour magnitude ratio diagram (TCMRD) approach is proposed to investigate the nature of extinction law and to reduce the stellar scattering of TCD. In this approach, the colour values of an individual star are normalized with respect to its magnitude. The normalized colour-ratio values are different from the normal colour ratio values, which is clearly verified through Tables 5 and 6. The resultant TCMRD of stellar clusters are shown in Fig. 6 (a)–(c).

The difference of normalized colour ratio and normal colour ratio seems to be high in the shorter wavelength

Table 6. The slopes of the $(H-\lambda)/H$ versus $(H-K)/H$ diagrams in the direction of the cluster.

Ratios / Cluster	ESO65-SC03	Turner 6	Teutsch 106
$\frac{(H-B_{ph})/H}{(H-K)/H}$	-16.05 ± 1.09	-10.91 ± 0.76	4.93 ± 2.67
$\frac{(H-R_{ph})/H}{(H-K)/H}$	-11.67 ± 1.04	-8.77 ± 0.58	-0.71 ± 4.13
$\frac{(H-I_{ph})/H}{(H-K)/H}$	-6.61 ± 0.52	-6.43 ± 0.68	-1.83 ± 2.26
$\frac{(J-H)/H}{(H-K)/H}$	2.09 ± 0.15	2.06 ± 0.08	0.07 ± 0.34
$\frac{(H-W_1)/H}{(H-K)/H}$	1.08 ± 0.09	1.54 ± 0.07	0.85 ± 0.29
$\frac{(H-W_2)/H}{(H-K)/H}$	0.87 ± 0.12	1.49 ± 0.08	0.73 ± 0.43

(λ) whereas this difference gradually decreases towards the infrared wavelength. Both ratio values seem to be identical for W_2 band. In the case of Teutsch 106, said ratio may be arising due to the stellar sub-sequence. To verify the reality of prescribed ratios of the Teutsch 106, the whole cluster region is adopted to estimate the colour ratios. Since, the resultant colour-ratios are abnormal, the sub-sequence is not responsible for the abnormal values of colour-ratios. Moreover, colour-ratio values of Teutsch 106 are abnormal for any one of I_{ph}, B_{ph}, R_{ph} or band, whereas similar values of TCR and TCMR are obtained for K, W_1 and W_2 bands. These deviated values of Teutsch 106 region is due to the large quantity of stellar dust and gas clouds within it. It seems through Tables 5 and 6 that the uncertainties of CMR values are decreased for ESO 65 03 and Turner 6 whereas in the case of Teutsch 106, uncertainties of CMR values are increasing according to normal color values. On this background, it is concluded that the stellar scattering is effectively reduced in TCMRD planes for the dust free cluster region, whereas it is increased for dust-affected cluster regions. Thus, the stellar scattering of TCMRD is directly depended on the amount of stellar dust.

6. Young stellar object fraction

The number of Young stellar objects (YSOs) within OCs is dependent on its age, and the YSO fraction of any cluster reduces with its evolution. We determine the free reddening parameter of each star by following the expression of Buckner & Froebrich (2013),

$$Q = (J-H) - \frac{E(J-H)}{E(H-K)} \times (H-K). \tag{6}$$

The value of $E(J-H)/E(H-K) = 1.55$ (Mathis 1990) is used for determining Q. YSOs are stellar objects having Q value less than -0.5 mag (Buckner & Froebrich 2013). The YSOs' fraction of a cluster is a ratio of the number of YSOs ($N_{\rm YSO}$) and the total number of cluster members ($N_{\rm cl}$). To reduce the photometric scattering in small number of YSOs within cluster, the YSOs fraction is estimated by the following relation (Buckner & Froebrich 2013):

$$Y_{\rm frac} = \frac{N_{\rm YSO} - \sqrt{N_{\rm YSO}}}{N_{\rm cl}}. \tag{7}$$

There are 7, 3 and 94 YSOs identified for $ESO65$ $SC03$, Teutsch 106 and Turner6 regions, respectively. Similarly, the $Y_{\rm frac}$ of these stellar clusters are found to be 0.026, 0.000 and 0.003 respectively. After comparison of our YSO fraction values with the 'Appendix A: FSR cluster property table' from Buckner & Froebrich (2013), we conclude that the low fractional values are found for Teutsch 106 and Turner 6 regions, whereas the average fraction value is obtained for the ESO65 SC 03.

7. Discussion and conclusion

The OCs are good tracer of galactic evolution process and star formation history. These studies are possible due to the precise measurement of their parameters. Since, the field stars (FS) of OCs reduces the precision in estimation of parameters, their decontamination (separation of cluster members) are needed. The said decontamination is carried out through the statistical cleaning approach (Joshi *et al.* 2015), which is based on the colours and magnitudes of the stars. Since, this approach is highly dependent on the adopted grid size around field stars, the decontamination of FS required some more attention. In addition, the identification of MS of the statistical cleaned $(J-H)/H$ CMD (refer

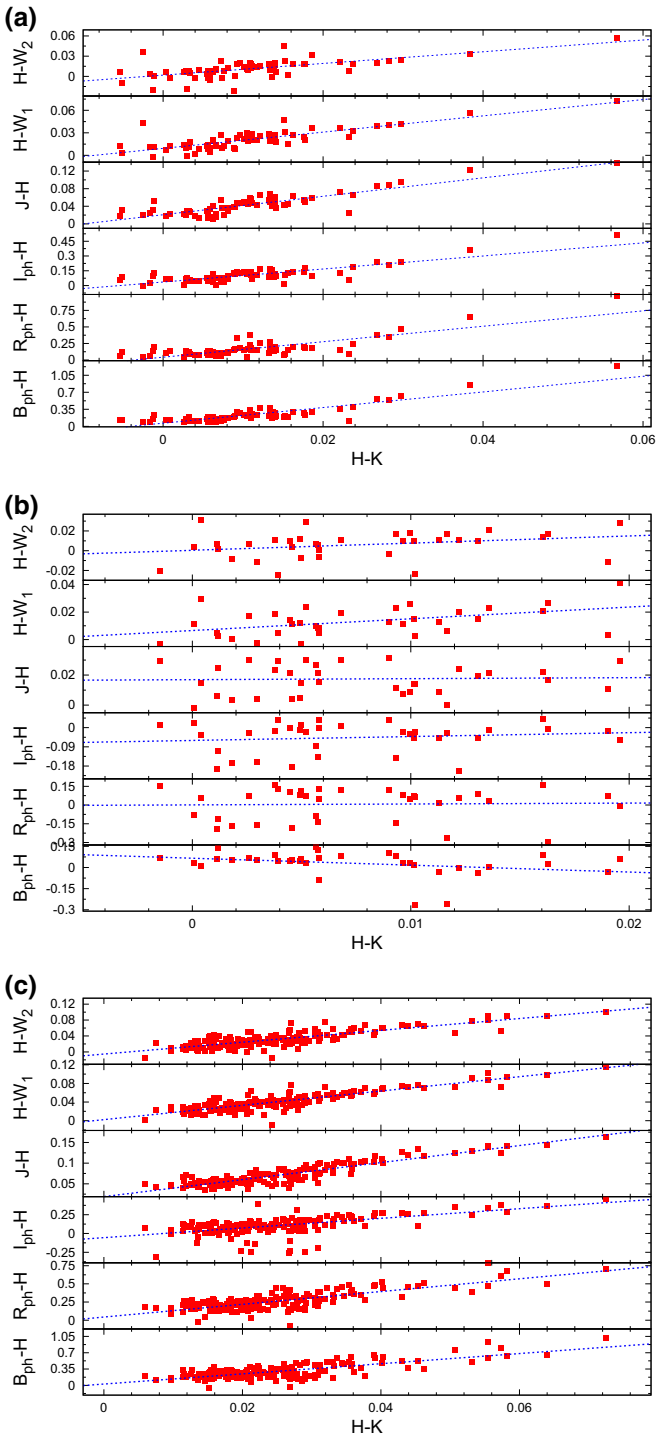

Figure 6. The two-colour magnitude ratio diagrams of cluster are shown here. (**a**) ESO65-SC03, (**b**) Teutsch 106 and (**c**) Turner 6.

Fig. 4(b)) is difficult due to non-fixed separation boundary of fainter stars within the CMD plane. This difficulty can be overcome through the CMRD approach. These separated stellar sequences are used to identify the MS of the cluster (e.g. Teutsch 106). The straight dividend line and stellar separation of the fainter stars are the main features of the CMRD, which is not possible on normal CMD plane. Such analysis will open a new window of identification of stellar clusters within embedded region of the Galactic disk and highly influence region of interstellar gases. The results of the spatial morphological parameters of each cluster have been summarezed in

Table 2. The different spatial parameters of studied stellar clusters are found through the extracted data sets from PPMXL catalogue and 2MASS catalogue. The prescribed parametric variation arises due to excess of listed fainter stars in PPMXL catalogue compared to 2MASS catalogue. The multi-band catalogue seems to be more effective with respect to catalogues of one or two bands. Since, the PPMXL catalogue also contains some false fainter stars, it is needed to verify the stellar nature before using it. On this background, we utilized the 2MASS catalogue for parametric analysis.

The distance, age and reddening of each cluster has been estimated by best fitted theoretical isochrones (based on model star radius, temperature and chemical composition) on $J-H$ vs. H and $H-K$ vs. H CMDs. The age, distance and reddening of $ESO65-SC03$ are found to be 0.56 ± 0.01 Gyr, 3.04 ± 0.30 kpc and 0.38 respectively. The distance and reddening of Turner 6 are estimated to be 3.12 kpc and 1.03 mag respectively. The age, distance, and reddening of Teutsch 106 are found to be 0.79 $\pm$ 0.05 Gyr, 1.73 kpc and 0.32 mag respectively. We found greater size of Teutsch 106 compared to Dias *et al.* (2014). These results are summarized in Table 4, the listed values are closed reddening values through $(J-K)/(J-H)$ TCD. The chang in the angular position of the stellar clusters' members leads to their proper motion. Since each member of the cluster has different proper motion values, mean proper motion of the cluster would be useful to understand the cumulative properties of members. The values of each cluster is summarized in Table 3. The nature of extinction law is varied within OCs due to the presence of interstellar gaseous/clouds/dust. The clour-ratio of stellar clusters are determined through the linear fits and listed in Table 5, whereas normalized colour-ratios have been summarized in Table 6. The variation between the values of normalized colour-ratio and normal colour ratio is higher for the shorter wavelength, whereas it decreases towards the higher wavelength.

The separated stellar-sequences of stellar clusters provide the crucial information about their evolution process. The constant value of normalized-colour ratios are used to separate the stellar sequences on CMRD plane. The colour-ratio values for Teutsch 106 through TCD and TCMRD are far away from the values of other stellar clusters due to the presence of inter-stellar dust or gases. The stellar scattering of TCMRD plane depends on the amount of associated interstellar-gaseous. Thus, the study of stellar sequences will become a milestone to identify the new stellar clusters. The stellar enhancement is not only a single property of the cluster, but an associate stellar sequence is more important to understand the spatial and dynamical morphology of the cluster.

Acknowledgements

The authors would like to thank Aayam Printers (Nanakmatta) for providing computer facilities, and also thank the SIMBAD and VIZIER services. We made use of data products from the Two Micron All Sky Survey, which is a joint project of the University of Massachusetts and the Infrared Processing and Analysis Center/California Institute of Technology, funded by the National Aeronautics and Space Administration and the National Science Foundation. We also made use of data products from the Wide-field Infrared Survey Explorer, which is a joint project of the University of California, Los Angeles, and the Jet Propulsion Laboratory/California Institute of Technology, funded by the National Aeronautics and Space Administration.

References

Bate, M. R., Bonnell, I. A., Bromm, V. 2003, *MNRAS,* **339**, 577.

Bonatto, C., Bica, E. 2010 *Astron. Astrophys.,* **521**, A74.

Bonatto, C., Bica, E., Ortolani, S., Barbuy, B. 2006, *Astron. Astrophys.,* **453**, 121.

Buckner, A. S. M., Froebrich D. 2013, *MNRAS,* **436**, 1465.

Bukowiecki, L., Maciejewski, G., Konorski, P., Strobel, A. 2011, *Acta Astron.,* 62.

Corradi, W. J. B., Maia, F. F. S., Santos-Jr. J. F. C. 2009, *Star clusters – Galactic Building Blocks throughout Time and Space*, Proceedings IAU Symposium No. 266.

Dias, W. S., Alessi, B. S., Moitinho, A., Lepine, J. R. D. 2002, *Astron. Astrophys.,* **389**, 871.

Dias, W. S., Monteiro, H., Caetano, T. C., Lepine, J. R. D., Assafin, M., Oliveria, A. F. 2014, *Astron. Astrophys.,* **564**, A79.

Dias, W. S., Monteiro, H., Caetano, T. C., Oliveria, A. F. 2012, *Astron. Astrophys.,* **539**, A125.

Fiorucci, M., Munari, U. 2003, *Astron. Astrophys.* **401**, 781.

Friel, E. D. 1995, *Ann. Rev. Astron. Astrophys.,* **33**, 381.

Froebrich. 2010, *MNRAS,* **409**, 128.

Girardi, L. *et al.* 2010, *Astrophys. J.,* **724**, 1030.

Harris, W. E., Pudritz, R. E. 1994, *Astron. J.,* **429**, 177.

Hasan, P. 2005, *Bull. Astr. Soc. India,* **33**, 151.

Hasan, P., Kilambi, G. C., Hasan, S. N. 2008, *Astrophys. Space Sci.,* **313**, 363.

Joshi, G. C., Tyagi, R. K. 2015, *6th International Conference on Recent Trends in Applied Physical, Chemical Sciences, Mathematical/Statistical and Environmental Dynamics (PCME-2015)*, pp. 37–42.

Joshi, G. C., Joshi, Y. C., Joshi, S., Tyagi, R. K. 2015, *New Astron.,* **40**, 68.
Joshi, G. C., Joshi, Y. C., Joshi, S., Chowdhury, S., Tyagi, R. K. 2015, *Publ. Astron. Soc. Australia,* **32**, 22.
Joshi, G. C., Tyagi, R. K. 2016, *MNRAS,* **455**, 785.
Joshi, Y. C., Balona, L. A., Joshi, S., Kumar, B. 2014, *MNRAS,* **437**, 804.
Kaluzny, J., Udalski, A. 1992, *Acta Astron.,* **42**, 49.
Kharchenko, N. V., Piskunov, A. E., Schilbach, E., Roëser, S., Scholz, R.-D. 2013, *Astron. Astrophys.,* **558**, A53.
Mathis, J. S. 1990, *Ann. Rev. Astron. Astro phys.,* **28**, 37.
Marigo, P. *et al.* 2008, *Astron. Astrophys.,* **482**, 883.
Morgan, D. H., Nandy, K. 1982, *MNRAS,* **199**, 979.
Peterson, C. J., King, I. R. 1975, *Astron. J.,* **80**, 427.
Roëser, S., Demleitner, M., Schilbach, E. 2010, *Astron. J.,* **139**, 2440.
Santos Jr., J. F. C., Bonatto, C., Bica, E. 2005, *Astron. Astrophys.,* **442**, 201.
Schild, R., 1977, *Astron. J.,* **82**, 337.
Schlegel, D., Finkbeiner, D., Davis, M. 1998, *Astrophys. J.,* **500**, 525.
Sharma, S., Pandey, A. K., Ogura, K., Mito, H., Tarusawa, K., Sagar, R. 2006, *Astron. J.,* **132**, 1669.
Sneden, C., Gehrz, R. D., Hackwell, J. A., York, D. G., Snow, T. P. 1978, *Astrophys. J.,* **223**, 168.
Tadross, A. L. 2009, *Astrophys. Space Sci.,* **323** Issue-4, 383.
Wright, E. L., Eisenhardt, P. R. M., Mainzer, A. K. *et al.* 2010, *Astron. J,* **140**, 1868.
Yadav, R. K. S., Sariya, D. P., Sagar R. 2013, *MNRAS,* **430**, 3350.
Zacharias, N., Finch, C. T., Girard, T. M., Henden, A., Bartlett, J. L., Monet, D. G., Zacharias, M. I. 2013, *Astron. J.,* **145**, 44.
Zhao, J. L., Shao, Z. Y. 1994, *Astron. Astrophys.* **288**, 89.